Feasibility Study on Liquid Divertor Using Molten Salt Free Surface Flow with Turbulent Promoters*)

Takahiro IJIMA, Shota SAKURAI, Fumiya TAKAHASHI, Shinji EBARA†)
and Hidetoshi HASHIZUME

Tohoku University, 6-6-01-2 Aramaki-Aza-Aoba, Aoba-ku, Sendai, Miyagi 980-8579, Japan

(Received 9 January 2023 / Accepted 20 June 2023)

A liquid Flibe divertor is proposed as a fusion DEMO reactor divertor that can suppress the surface temperature with low velocity through turbulent promoters, which are necessary considering the low heat transfer performance of liquid Flibe. Using water as a simulant fluid, a pebble-sunk structure (PSS) is introduced herein as a turbulent promoter. The heat transport characteristic is evaluated by flow visualization and heat transport experiments. The experimental results show that the kinetic energy and the heat transport near the free surface are enhanced when the PSS is introduced.

Keywords: fusion reactor, divertor, liquid divertor, molten salt divertor, turbulent promoter, PSS

DOI: 10.1585/pfr.18.2405075

1. Introduction

A liquid metal divertor is proposed as a fusion reactor divertor [1]. Compared with solid divertors, a liquid divertor is unaffected by the maximum heat load and the edge localized modes [2]. One feature of a liquid divertor is that it can prevent damage to the plasma-facing surface. Nevertheless, using liquid metal in a divertor frequently leads to the problem of an extremely large magnetohydronamic (MHD) effect, which mainly appears as the pressure drops due to high electrical conductivity. By contrast, the MHD effect generated in a liquid Flibe divertor using molten salt, Flibe, can be suppressed because of its low conductivity. In addition, the vapor pressure of liquid Flibe is low, making it possible to suppress the particle contamination into the plasma. However, liquid Flibe has a low heat transport performance due to its high Prandtl number. Therefore, it may be very difficult to remove the heat load near the free surface, which may possibly cause an excessive evaporation of Flibe. Improving the heat transport performance caused by the increased flow velocity is limited by the pump power and the electrolysis of Flibe. Therefore, using liquid Flibe as a divertor necessitates an enhanced heat transport performance without flow velocity increase.

The usage of a sphere packed pipe (SPP) was proposed to enhance the heat transfer performance of an enclosed Flibe channel flow. The previous studies [3–5] used SPP to prove the improvement of the heat transfer performance and evaluate the mechanism. With reference to the SPP, the pebble-sunk structure (PSS) is introduced in this work as a turbulence promoter. In the PSS, pebbles (spheres) are set on the bottom of an open channel (Fig. 1).

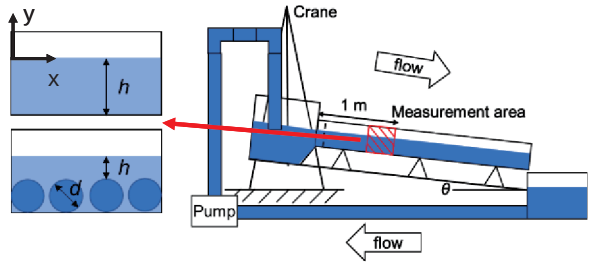

Fig. 1 Schematic of the experimental apparatus.

This work aims to experimentally demonstrate the feasibility of heat transport enhancement near the free surface using the PSS as a turbulence promoter in a low-flow velocity region of an open channel. Flow visualization and heat transport experiments are conducted to evaluate the turbulence flow characteristic and the heat transport performance near the free surface, respectively. The results are compared with those obtained in an open channel with a smooth bottom. Lastly, the effect of the PSS to the turbulent flow and the thermal field in the channel are discussed minutely.

2. Experimental System and Setup

2.1 Flow visualization experiment

Figure 1 illustrates the experimental setup in this work. The test section is a straight open flow channel 190 mm in width and 2 m in length. The measuring section is located 1 m downstream of the channel inlet. The experimental apparatus made it possible to keep the liquid film thickness constant under each experimental condition by changing the flow channel inclination in the measuring section. The working fluid was water. Table 1 presents the experimental conditions in this study, where U is the mean

†) *Corresponding author's e-mail: shinji.ebara.e6@tohoku.ac.jp*
*) This article is based on the presentation at the 31st International Toki Conference on Plasma and Fusion Research (ITC31).

Table 1 Bottom, velocity conditions.

	U (m/s)	Re (-)	h (mm)	d (mm)	θ (deg)
case1	0.26	7654	30	0	0.05
case2	0.53	14365	27	0	0.45
case3	0.25	7578	30	40	0.10
case4	0.49	14807	30	40	1.95

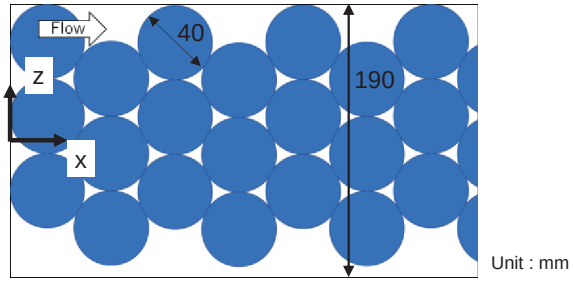

Fig. 2 Pebble arrangement in the PSS.

velocity; h is the liquid film thickness; Re is Reynolds number based on U and h; and d is the pebble diameter. The pebbles in the PSS were placed in a staggered arrangement (Fig. 2). The fluid flow in each case was measured through particle image velocimetry (PIV) using FIREFLY 300 W (Oxford Lasers) as a diode laser, HAS-D72 (DITECT) as a high-speed camera, and Vid PIV 4.6 (Oxford Lasers) as an analysis software. The laser sheet was irradiated at the center of the flow channel to observe the flow field without the influence of the channel's side walls. In a single measurement, the camera captured 2000 images (1000 pair images), and 1000 velocity data (instantaneous value) were obtained. The camera resolution was 1280×1080 px. The frame rate of each pair image was 250 fps. In this experiment, a 4 s flow field was recorded in one measurement. The considerations presented here indicated that this was long enough for the present experimental conditions. One can roughly estimate the largest timescale in the flow (i.e., ~0.1 s at most) by using the largest velocity, length scales, time-averaged velocity, and liquid film thickness in the experiment. Another method is estimation using the Strouhal number (St), which considers the periodic fluctuations in the flow that occur downstream of the object. Accordingly, $St \sim 0.2$ in a wide range of Re; hence, the largest frequency in the experiment flow could be estimated as approximately 2 Hz, and the largest timescale was ~0.5 s. Using the obtained instantaneous velocity data, the time-averaged velocity in the x and y directions ($\bar{u}$, $\bar{v}$) and the velocity fluctuation (u', v') were calculated as follows:

$$\bar{f} = \frac{1}{\Delta t}\int_0^{\Delta t} f \, \mathrm{d}t,$$
$$f' = f - \bar{f},$$

where f is the instantaneous value of the velocity data (u, v). The kinetic energy in the visualization plane (k) was calculated as follows from the obtained velocity fluctuations:

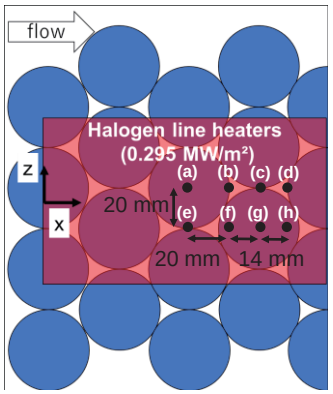

Fig. 3 Temperature measurement area in the x and z directions.

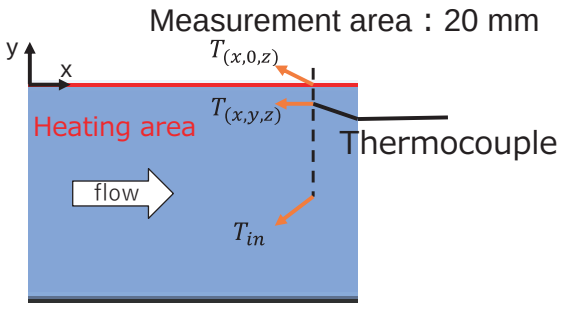

Fig. 4 Temperature measurement area in the y direction.

$$k = \frac{1}{2}\left\{\overline{(u')^2} + \overline{(v')^2}\right\}.$$

2.2 Heat transport experiment

A heat transport experiment was conducted using halogen heaters as the heat source for the surface heat load. In this experiment, four 900 W halogen heaters were used to provide 0.295 MW/m^2 heat load to the free surface. Subsequently, 0.5 mm-diameter type-K thermocouples were used for the temperature measurement. Figure 3 shows that the temperature measurements for the x and z directions were conducted on the representative positions of the PSS. The measurements in the y direction (Fig. 4) were taken at 0.1 mm intervals near the surface and 1.0 mm in the "bulk" water for 20 s. The temperature rise, ΔT, and the root mean square of the temperature fluctuation, T_{rms}, near the free surface were calculated as follows using the obtained temperature data:

$$\Delta T = \bar{T} - T_{in},$$
$${T_{rms}}^2 = \frac{1}{\Delta t}\int_0^{\Delta t} (T')^2 \, \mathrm{d}t,$$

where $\bar{T}$ is the time-averaged value of the instantaneous measured temperature; T and T' denote the temperature fluctuations obtained from the same manner of velocity fluctuation; and T_{in} is the inlet temperature. In the experiment, the free surface position must be determined. This was visually difficult to do so due to the slight rippling; hence, the measured temperature was used to evaluate the surface position. When the thermocouples were out of the

water, the halogen heaters heated the thermocouples directly, resulting in very high temperature measured. Therefore, the free surface was defined as the area between the positions where the measured temperatures exceeded and not exceeded 100°C.

3. Results and Discussion

3.1 Flow visualization experiment

The PIV validity in this experiment was approximately 90% for cases 1 and 4 and approximately 75% for cases 2 and 3. Cases 2 and 3 were less valid due to the lower measurement accuracy near the free surface.

Figure 5 shows the velocity distributions for all cases, where 0 in the vertical axis corresponds to the free surface position, and the vector notations are expressed by making the velocity component in the depth direction (y) 20 times larger. The flow vector was almost parallel to the flow direction throughout the measurement area in cases 1 and 2, with a smooth bottom surface. In contrast, in cases 3, and 4 with the installed PSS, the depth direction component periodically increased due to the flow disturbance by the pebbles.

Figure 6 depicts the turbulent kinetic energy distributions for all cases. The turbulent kinetic energy was normalized by the time-averaged mean velocity. The PSS installation in the channel resulted in a higher turbulent kinetic energy compared to that obtained in the smooth bottom channel under the same flow velocity. In other words, the PSS may be thought to indeed act as a turbulence promoter.

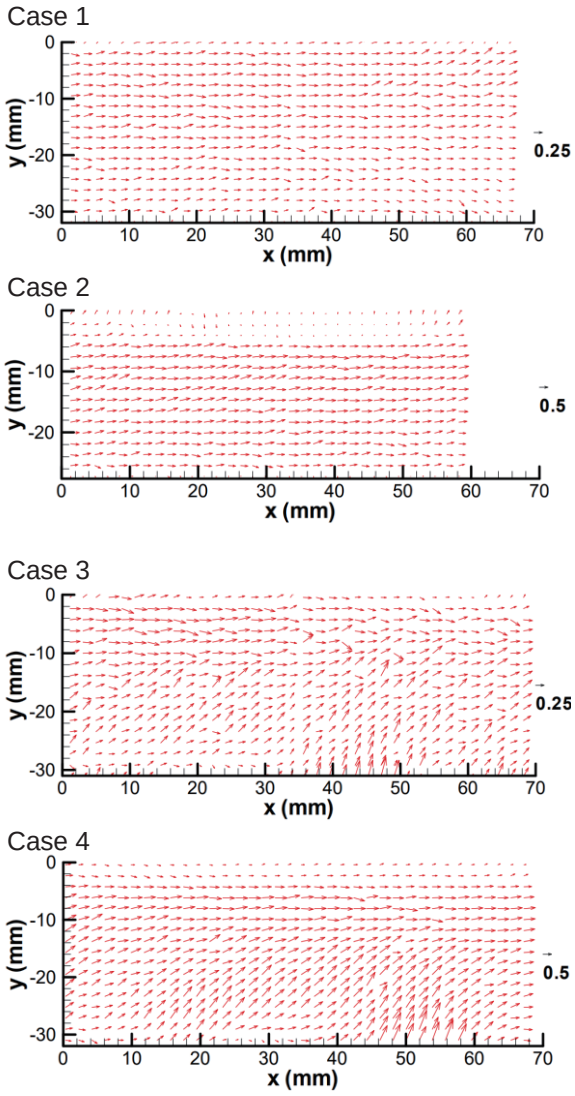

Fig. 5 Flow velocity distribution.

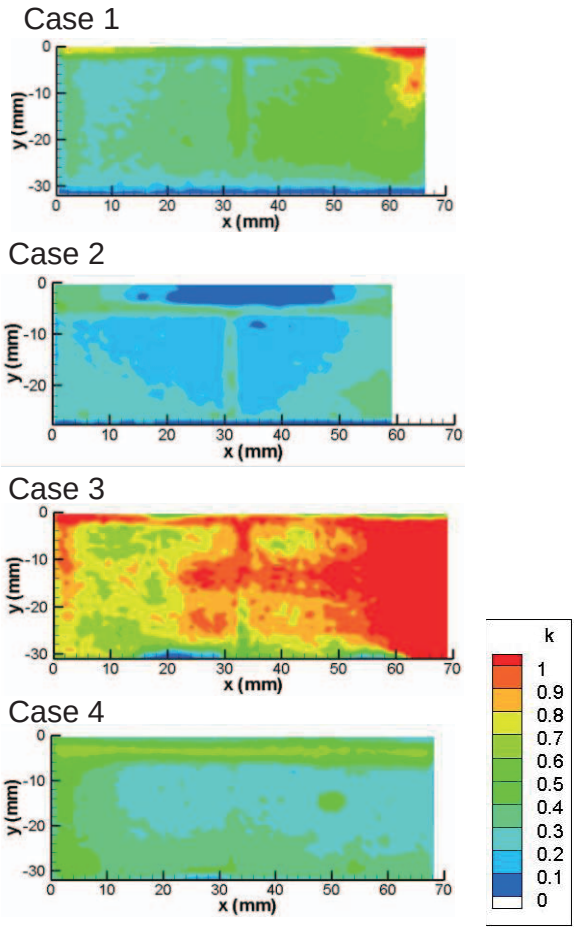

Fig. 6 Kinetic energy distribution.

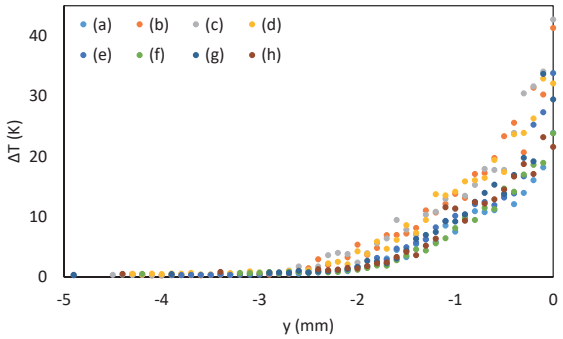

Fig. 7 Temperature rise comparison by measurement.

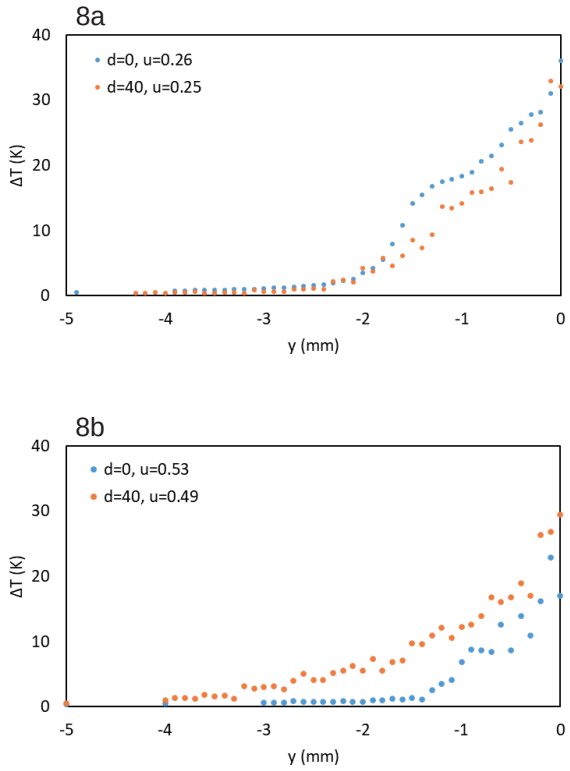

Fig. 8 Temperature rise comparison.

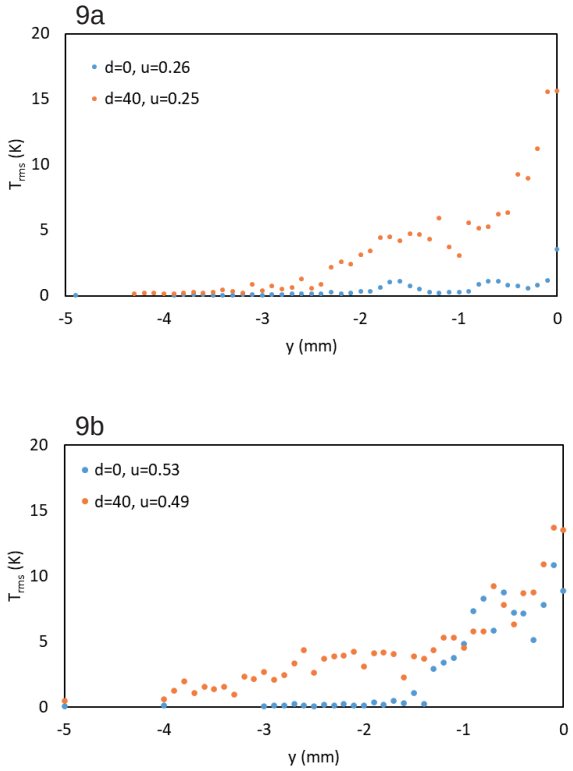

Fig. 9 Temperature fluctuation comparison.

3.2 Heat transport experiment

Figure 7 illustrates the temperature rise at each measurement position in Case 3, where the legends correspond to the positions expressed in Fig. 3. The temperature rise depicted in (a) was more limited to the location near the free surface compared to that in (b) to (d) because the data in (a) were obtained in the most upstream part of the channel and among all the data, and the thermal boundary layer was still developing. The temperature rise indicated in (e) to (h) was smaller than that in (a) to (d) because the amount of heat received on the free surface was thought to become smaller when the measurement position in the z direction was changed. Hereafter, the temperature data obtained at (d) were chosen as the reference and discussed.

Figure 8 compares the temperature increases near the free surface at each flow velocity with or without the PSS. Figure 8a (low flow velocity) shows no significant difference in ΔT. By contrast, ΔT in the PSS channel was slightly larger than that in the smooth channel. In Fig. 8b (high flow velocity), ΔT in the PSS channel was larger in the whole region. These results indicate that the PSS promoted turbulence and enhanced the heat transport performance, especially in the high-flow velocity case.

Figure 9 compares the temperature fluctuations between the cases with or without the PSS at each flow velocity. In the case of a smooth channel, the temperature fluctuation increased only in a very limited region near the free surface. By contrast, the temperature fluctuation in the liquid near the free surface increased because the introduction of the PSS increased the heat transport in the liquid. Consequently, the heat received at the surface can be transported deeper into the liquid by introducing the PSS.

4. Conclusion

In this study, the heat transport performance in the channel with the PSS as a turbulence promoter was evaluated through flow visualization and heat transport experiments. The flow visualization experiment showed that the PSS enhanced the turbulence flow not only near the bottom structure, but also near the free surface. The heat transport experiment also demonstrated that the PSS enhanced the heat transport performance near the free surface in both the low- and high-flow velocity cases. This led to the liquid divertor suppressing the temperature at the liquid surface at a lower flow velocity. The future work will include the improvement of the measurement accuracy near the free surface to evaluate the heat transport performance in more detail.

Acknowledgment

This work was supported by JSPS KAKENHI Grant Number JP19H01871.

[1] B. Badger *et al.*, "UWMAK-I-A Wisconsin Toroidal Fusion Reactor Design", UWFDM-68 (1974).
[2] Y. Kamada *et al.*, Plasma Fusion Res. **82**, No.9, 566 (2006).
[3] M. Varahasamy *et al.*, Int. J. Heat Mass Transfer **39**, No.18, 3931 (1996).
[4] A. Watanabe *et al.*, Fusion Eng. Des. **88**, 1357 (2013).
[5] S. Ebara *et al.*, Fusion Eng. Des. **89**, 1251 (2014).